PCCP

Accepted Manuscript

ROYAL SOCIETY OF CHEMISTRY

www.rsc.org/pccp

High voltage and efficient bilayer heterojunction solar cells based on organic-inorganic hybrid perovskite absorber with low-cost flexible substrate

Yi-Fang Chiang[a], Jun-Yuan Jeng[a], Mu-Huan Lee[a], Shin-Rung Peng[a], Peter Chen[a,b,c*], Tzung-Fang Guo[a,b*], Ten-Chin Wen[d], Yao-Jane Hsu[e], Ching-Ming Hsu[f]

[a)] Department of Photonics

[b)] Advanced Optoelectronic Technology Center (AOTC)

[c)] Research Center for Energy Technology and Strategy (RCETS)

[d)] Department of Chemical Engineering

National Cheng Kung University

Tainan 701, Taiwan

[e)] National Synchrotron Radiation Research Center

Hsinchu 300, Taiwan

[f)] Department of Electro-Optical Engineering

Southern Taiwan University

Tainan 701, Taiwan

Corresponding author

Peter Chen email: petercyc@mail.ncku.edu.tw

Tzung-Fang Guo email: guotf@mail.ncku.edu.tw

Keywords: $CH_3NH_3PbI_3$, organometal halide perovskite, heterojunction solar cell, fullerene, flexible electronics

Abstract

A low temperature (<100 °C), flexible solar cell based on organic-inorganic hybrid $CH_3NH_3PbI_3$ perovskite/fullerene planar heterojunction (PHJ) is successfully demonstrated. In this manuscript, we study the effects of energy level offset between solar absorber (organic-inorganic hybrid $CH_3NH_3PbI_3$ perovskite) and the selective contact materials on the photovoltaic behaviors for the planar organometallic perovskite/fullerene heterojunction solar cells. We find that the difference between the highest occupied molecular orbital (HOMO) level of $CH_3NH_3PbI_3$ perovskite and the Fermi level of indium-tin-oxide (ITO) dominates the voltage output of the device. ITO films on glass or on the polyethylene terephthalate (PET) flexible substrate with different work functions are performed to illustrate the phenomenon. The higher work function of the PET/ITO substrate decreases the energy loss for hole transfer from the HOMO of perovskie into ITO and minimizes the energy redundancy for photovoltage output. The devices using the high work function ITO substrate as contact material show significant open-circuit voltage enhancement (920mV), with the power conversion efficiency of 4.54 %, which represents the potential for low-cost and lightweight advantages of this type of extra-thin planar bilayer heterojunction solar cell.

Introduction

Cost-affordable and sustainable photovoltaic materials are vital for the future contribution of renewable solar energy supply to satisfy global energy demand. Low-cost devices such as dye-sensitized solar cells (DSCs)[1, 2], organic bulk heterojunction solar cells[3] (OPVs) and other solution process compatible devices are considered as potential candidates for the future emerging photovoltaic technologies.[4] It is important to develop new photovoltaic devices that fulfill the requirements with thin-film absorber, nontoxic and earth-abundant materials, low-energy manufacturing process and cost affordable for effective sustainability. Organic-inorganic hybrid organometal halide perovskites, which found applications in thin film field-effect transistors[5], have drawn massive attentions for photovoltaic applications recently due to their excellent performances as light absorber and carrier transporter.[6-8] Photovoltaic devices based on this material delivering power conversion efficiency (PCE) between 12~15% have been reported recently[9-13]. With optical band gap around 1.5 eV, organometal halide perovskites are intrinsically optimal solar absorbers for high efficiency according to the Shockley–Queisser limits.[14] Moreover, its high extinction coefficient over the visible spectrum and low exciton binding energy make it a superior light harvester for photovoltaic application within nano-scale.[15-18] It was estimated that optimized efficiency of 20 % is expectable for perovskite based solid-state solar cells in a perspective report.[19] One merit of the perovskite solar cell is the high output voltage close to the optical band gap which reduced the energy redundancy that exist in most excitonic-solar cells like OPV or DSCs.[8, 11, 20, 21] Since perovskite behaved ambipolar conduction and worked as either electron or hole transporter, this allows versatile design of device architectures. For example, Bi *et al.* used perovskite as electron transporter to form a junction in contact with various hole transport materials (HTMs).[22] Lee *et al.*, deposited perovskite on the surface of

meso-structured Al_2O_3 layers where the Al_2O_3 acts as a non-injecting electrodes scaffold and perovskite as electron transport medium respectively.[8] Kim *et al.* compared the perovskite cells made with TiO_2 and ZrO_2 as hosting electrodes and showed that charge accumulation in perovskite is mainly responsible for the photovoltaic function.[23] A two-step deposition technique in preparing perovskite thin film showed that non-injecting ZrO_2 mesoscopic host with higher photovoltage and longer electron lifetime indicating the intrinsic transport characteristic in peroskite material itself.[24] Recently, highly efficient thin film flat junction without mesocopic nanostructure has been reported implying relatively long electron diffusion in perovskite.[10, 25] In these cases, the absorber/HTM contact acts as a selective interface to facilitate hole injection while perovskite layer remained as an electron-transporting medium. On the contrary, Etgar *et al.* observed that the perovskite can play the role of light harvester and hole conductor by applying it in contact with electron acceptor (TiO_2) to realize a charge separation junction.[26, 27] Our previous results also demonstrated that the perovskite/fullerene interface has the similar function to dissociate excitons as the planar donor-acceptor junction and the perovskite served as light absorber and hole transporting phase[28]. Another category of device architecture is a structure analogous to DSCs in which the perovskite layer behaved as light absorbing pigments. The thin layer of light harvester is sandwiched between electron and hole transporter where both electron and hole transfer can take place at the selective contacts.[7, 9, 11, 18, 29] Charge separation characteristics between perovskite and various kinds of hole transport materials have been scrutinized lately and showed extremely high yield for many HTMs.[11, 20, 21] A critical issue remained to be tackled for the perovskite absorber is the balance between light absorption and charge collection. From the optical property, it seems to be that a very thin layer within few hundreds nano meters is capable to saturate light harvesting. Providing the charge

diffusion length is longer than this feature size, mesoporous electrode that intended to increase optical cross section may not be required. Various device structures attempted to reduce the electrode surface area, such as nanosheet[26], nanorods[29, 30], nanowire[31], nanofiber[32] have been realized and delivered promising photovoltaic conversion efficiency. Moreover, high performance PHJ perovskite solar cells have been realized using either solution process or vapor deposition method[10, 25]. These results suggested that the thin film PHJ is a suitable device configuration for organic-inorganic perovskite based material. Some of the most recent solar cells using organometal halide perovskites are summarized in Table 1 with the device architectures, the role of perovskite, and their photovoltaic performances outlined. It is worth noting that the ratio of voltage output versus the optical band gap for efficient perovskite devices is close to 65~69 %, which is fairly high in the emerging photovoltaic devices.[33]

Recently, we have proposed the design of $CH_3NH_3PbI_3$ perovskite/fullerence planar-heterojunction hybrid solar cells that applied extremely thin absorber with thickness of 30 nm.[28] By judicious selections of electron acceptor materials, we found that the charge separation between $CH_3NH_3PbI_3$ perovskite and fullerence derivatives is very efficient and the lowest unoccupied molecular orbital (LUMO) level of the acceptor layer dominates the photovoltage output. We observed that the higher LUMO level increases the open-circuit voltage (V_{OC}) and the efficiency of the device, which is a result of decreased charge separation energy cost. Although the efficiency is not as high as those devices made of mesoporous electrodes (which mainly due to the lower optical cross section) or thicker thin film device, the facile, simple and low-temperature processes are advantageous for cost viable solar cells using plastic substrates. Our interesting results avoid using high temperature procedure, which is inevitable for devices using oxide mesoscopic or underlayer in cell structure. In this

report, we further improve the photovoltaic performances through judicious selection of energy level matching on contact materials. Using the substrate with lower energy loss between the light absorber and contact material, we remarkably increased the V_{OC} from 0.50 to 0.92 *V*, with PCE enhanced to 4.54%.

Experimental

Materials preparation: The precursor solution of methyl ammonium iodide (CH_3NH_3I) and lead iodide (PbI_2) were prepared as reported elsewhere [8, 26, 28].

Fabrication of $CH_3NH_3PbI_3$ perovskite/fullerence hybrid solar cells: The two indium-tin-oxide (ITO) substrates are glass/ITO from RITEK Corp (15 Ω/□, denoted as the ITO-1) and the flexible polyethylene terephthalate (PET)/ITO from Optical Filters Ltd (15 Ω/□, denoted as the ITO-2). Another nickel-doped ITO (Ni-ITO) substrate was prepared by sputtering a 15 nm on ITO-1 substrate. ITO structures were patterned, cleaned, and spin coated with conductive polymer, poly(3,4-ethylenedioxythiophene) poly(styrenesulfonate) (PEDOT:PSS) (Baytron P, Bayer AG, Germany). The ethylammonium lead iodide ($CH_3NH_3PbI_3$) extra-thin perovskite layer is deposited on ITO/PEDOT:PSS surfaces by spin coating. The glass/ITO/PEDOT:PSS substrates were pre-heated at 60 °C for 5 min then spin-casting $CH_3NH_3PbI_3$ in γ-butyrolactone solution (14.9 wt.%) at 6000 rpm for 30 seconds. The preheating treatment of the substrate ensures the evaporation of the solvent in a fast manner and inhibits the coarsening of the crystals. The coated layer was annealed at 100°C for 15 min to receive dark brown $CH_3NH_3PbI_3$ thin film. The fullerene (C_{60}) (30 nm) (>99.5%, Aldrich), [6,6]-phenyl C61-butyric acid methyl ester (PCBM) (> 99%, Solenne, Netherlands), bathocuproine (BCP) (Aldrich) (10 nm) and aluminum (Al) (100 nm) were deposited on the substrate inside a vacuum chamber (10^{-6} Torr) by thermal evaporation. C_{60} or PCBM is an acceptor layer forming a

junction with $CH_3NH_3PbI_3$ where the charge separation takes place. The thin BCP film acts as an exciton- or hole-blocking layer (EBL or HBL). C_{60} or PCBM and BCP layers are sequentially evaporated on the $CH_3NH_3PbI_3$ perovskite. The device was completed by thermal evaporation of Al as a negative electrode. The energy level diagram of device (PCBM as the acceptor) is illustrated in Scheme 1(a). The configuration of device architecture and a photo of the flexible device fabricated on PET/ITO (ITO-2) substrate are illustrated in Scheme 1(b).

We used quartz crystal to monitor the thickness for the evaporation process. The active area of the device is 0.06 cm^2 defined by a mask. All the procedures are implemented inside a nitrogen-filled glove box with oxygen and moisture levels less than 1 ppm except for casting the PEDOT:PSS layer (in atmosphere).

Characterization: Device characteristics, current density-voltage (*J-V*) curves, were measured in a nitrogen-filled glove box using a Keithley 2400 sourcemeter under the standard 1 Sun AM 1.5 G simulated solar irradiation (100 mW/cm^2) from Newport 91160A 300 W Solar Simulator (Class A). The simulated solar irradiance is corrected by a Si diode (Hamamatsu S1133) equipped with a Schott visible-color glass filter (KG5 color filter)[34]. The series resistance (R_S) and parallel resistance (R_P) are calculated by the method reported by Waldauf *et al.*[35]. The incident photon to electron conversion efficiency (IPCE) spectra were measured by a system composed of a 300 W xenon light source (Oriel), an Oriel Cornerstone 130 1/8 m monochromator, a Keithley 2400 sourcemeter, a chopper (Stanford research system Inc.) and a Lock-in amplifier (SR510, Stanford research system Inc.). UV-vis spectra were taken by a spectrometer (U4100, Hitachi). The high-resolution scanning electron microscopy (SEM) images were performed by a FEI Quanta 400. The work functions of ITO-1 and ITO-2 were measured by UV photoelectron spectroscopy (UPS) with He source of incident energy of 21.21 eV (He I line) in National Synchrotron Radiation

Research Center, Taiwan.

Results and Discussions

Figure 1(a) shows the current-voltage (*J-V*) characteristic curves of hybrid organic solar cells made of different positive electrodes, glass/ITO (ITO-1) and PET/ITO (ITO-2), respectively, with C_{60} derivatives as electron acceptor under AM 1.5 G, 100 mW/cm^2 simulated solar irradiation. Their detailed photovoltaic characteristics are shown as Table 2. In Figure 1(a), the device with the ITO-1 as the positive electrode and C_{60} as the electron acceptor (device 1) delivered V_{OC} of 0.60 V, short-circuit current density (J_{SC}) of 6.12 mA/cm^2, fill factor (FF) of 0.52, and PCE of 1.93 %. However, in the device 2 (ITO-2 as the positive electrode and C_{60} as the electron acceptor), it shows a dramatically enhanced power conversion efficiency of 3.62%, which is higher than that of device 1 due to its higher V_{OC} of 0.84 V and J_{SC} of 8.18 mA/cm^2. It is encouraging that the photovoltaic activity has significant improvement in the PCE using the flexible plastic PET/ITO (ITO-2) substrate, especially the higher V_{OC} and J_{SC}. To address the relationship between work function and V_{OC} in a more systematic manner, we use a substrate with chemically dope Ni-ITO (device 3) which possesses higher work function than ITO-1.[36, 37] The result is presented in Figure 1 (a) showing a relative higher V_{OC} than device made of ITO-1. This demonstrates that the manipulation of ITO work function by intentional chemical doping could effectively influence the voltage output. To avoid the influences of morphology on the photovoltaic performance, we performed the SEM images (Figure S1) of perovskite coated on the two substrates to show the difference in morphology is minor. The UV-vis absorption spectra (Figure S2) showed that the perovskite loading is slightly higher on PET/ITO substrate resulted in a general higher short-circuit current in devices made of ITO-2 with respect to ITO-1. The SEM

images and UV-vis spectra are available in the supplement information.

In general, the V_{OC} in solar cell devices can be regarded as the different quasi Fermi level measured at the terminal under light illumination ($V_{OC} = E_{F,n} - E_{F,p}$). The origin of V_{OC} in organic planar or bulk heterojunction solar cells is typically described either by the difference between the highest occupied molecular orbital (HOMO) level of the donor and the LUMO level of the acceptor ($\Delta E_{D\text{-}A} = HOMO_D\text{-}LUMO_A$) or by the work function difference ($\Delta \Phi_{electrodes}$) defined by the metal-insulator-metal (MIM) model [38-44]. For electrodes that form ohmic contact with the active layer, the V_{OC} is mainly determined by the donor-acceptor interface energy gap ($HOMO_D\text{-}LUMO_A$). It has been reported that the work function of cathode metal has only marginal effects on the change of V_{OC} unless surface modification layers are inserted between the acceptor and cathode[38, 45, 46]. For non-ohmic contact, the V_{OC} is mainly controlled by the work function difference between the electrodes as predicted by the MIM model. However, it is worthy to notice that some other effects such as morphology control or the oxidation potential of the donor conjugated polymers could have influences on the voltage as well[47, 48]. In our previous study, we found the LUMO level of the acceptor can manipulate the voltage value of perovskite/fullerene planar junction cell, which is expected from the interface energy gap model that the V_{OC} is governed by the $\Delta E_{D\text{-}A}$. An extra high voltage (1.3 V) device has been realized by judicious selection of perovskite and hole conducting material based on this reasoning[21]. A recent study on the doping effect of organic-inorganic perovskite showed that proper doping can enhanced the conductivity on HTM together with the output voltage due to the lowering (more positive shift) on the redox potential in 2,2'7,7'-tetrakis-(*N*,*N*-di-*p*-methoxyphenyl-amine)-9,9'-spirobifluorene (*spiro*-OMeTAD).[49] This also reflects the energy gap after charge separation can significantly dominate the voltage performance.

In this study, we used two ITO substrates and observed significant variation in the photovoltaic performances. We suspected that the main difference of the two materials is from the energy level of the work function. To understand the phenomenon, we conducted the UPS to determine the work function of ITO-1 and ITO-2 as presented in Figure 2. The ITO-1 and ITO-2 were probed by UV source (21.21 eV, He I line.). We observed the signal that indicates the edge of Fermi level (E_i) started at 1.11 eV and 1.62 eV with the cut-off energy ($E_{cut\text{-}off}$) of 17.52 eV and 17.63 eV for secondary electrons in Figure 2 for ITO-1 and ITO-2, respectively. For each sample, the work function is calculated from the UPS spectra by subtracting the energy of the incident beam with the width of the emitted electron between the onset of low-energy secondary electrons and the Fermi edge. The work function is estimated by the following equation[50, 51]:

$$\Phi = 21.21 - (E_{cut\text{-}off} - E_i)$$

We received the work functions of ITO-1 and ITO-2 are 4.8 eV and 5.2 eV respectively. By the UPS measurement, the ITO-2 has the higher work function of 0.4 eV than ITO-1. The holes transfer from the HOMO of perovskite to the highly conductive PEDOT:PSS with very small difference on work function, and the interface is considered to be ohmic without barrier for hole injection. Since the work function of ITO-2 is 0.4 eV higher than ITO-1, which results in closer alignment between photovoltaic active layer and contact material and reduces the energy loss for hole transfer between the HOMO level of perovskite and Fermi level of ITO-2. We attributed the increased V_{OC} in the ITO-2 device to this reduced energy gap. Lo *et al.* have reported that the V_{OC} of organic photovoltaic devices are governed by the work function differences between electrodes if the $\Delta\Phi_{electrodes}$ value between the two contact materials falls within a certain range (0 ~ -3 eV).[43] On the other hand, the influences of the anode contact work function on the output V_{OC} has been identified

with hole selective and non-selective contacts recently[52]. They found that the V_{OC} increases as the anode work function becomes larger. Considering our device using perovskite as donor in comparison with these reports, we found similar tendency for the dependences of V_{OC} on the work function of contact materials (ITO-1 and ITO-2) used in the anode. Our results suggested that the redundancy of hole injection into the contact electrode can be effectively reduced by choosing a conducting material with Fermi level close to the HOMO level of perovskite. The photovoltaic action is the capability to separate photoinduced charges and accumulate them with different chemical potential asymmetrically. As reported by Kim *et al.*, perovskite has high capacitance and the ability to accumulate charges itself leading to controlling the quasi Fermi level upon illumination.[23] Examine those high V_{OC} photovoltaic devices based on perovskite materials as summarized in Table 1, if the perovskite acts as an absorber and charge (either electron or hole) carrier, the voltage output is expected to be high since some charge transfer energy loss is saved compared to the sensitization or donor-accepter type devices. For the current type of device architecture, we believe it is important to select energetic favorable contact materials with work function well aligned to the HOMO of perovskite to maximize the energy output. One credit of our current study using the organometallic perovskite material in the OPV-like structure is its superior high voltage output compared with the other emerging photovoltaic technologies, such as OPV or DSCs, which suffered from high exciton binding energy (in OPV [53]) or charge transfer driving force (in DSCs[33, 54]). The perovskite material is known for its very low exciton binding energy, which is advantageous for charge separation. Our results further suggested that the energy level of contact materials could have strong impacts on the deliverable energy of photoinduced charges. The strategy and design of this novel layer architecture manifested that applying perovskite absorber in an OPV-like structure can significantly reduce the gap between

optical bandgap and photovoltage output which existing as the major deficit in OPV.

Our previous studies have reported that applying the acceptor material with relatively higher LUMO level in a planar $CH_3NH_3PbI_3$-based PHJ could increase the magnitude of V_{OC} and the efficiency.[28] It is noted that photovoltaic performance of $CH_3NH_3PbI_3$ perovskite/C_{60} or C_{60} derivatives PHJ are controlled the level position offset of donor and acceptor. Thus, for further enhancing the efficiency of device 2, we use PCBM (with higher LUMO level compare with C_{60}) to replace C_{60} in the application of the devices using ITO-2 as positive electrode. Figure 1(b) presents the *J-V* characteristic curves of hybrid organic solar cells made of PCBM as the acceptor in the PHJ using the ITO-1 and ITO-2 as positive electrode. The corresponding photovoltaic performances are summarized in Table 2. The device 4 applying PCBM (its LUMO level of -3.9 eV is higher than that of C_{60}, -4.5 eV) as the acceptor and ITO-1 as positive electrode exhibits V_{OC} of 0.75 V, J_{SC} of 4.8 mA/cm^2, *FF* of 0.59, corresponding to a PCE of 2.12% under standard AM 1.5 simulated solar irradiation. It can be observed that applying an acceptor with higher LUMO level could elevate the magnitude of V_{OC} from 0.60 V to 0.75 V comparing device 1 and device 4. A similar phenomenon is expected for device 2 and device 6 that use ITO-2 as anode material. The device using ITO-2 as positive electrode and PCBM as acceptor resulted in higher V_{OC}, J_{SC}, and PCE of 1.06 V, 6.2 mA/cm^2, and 3.13%, respectively, whereas lower FF, 0.47. The poor FF may be caused by the larger R_S due to the thicker thickness of PCBM for device 6. For this reason, the thickness of PCBM was reduced to 20 nm as the acceptor for device 7, which exhibits a V_{OC} of 0.92 V, J_{SC} of 7.93 mA/cm^2, FF of 0.62, leading to a maximum PCE of 4.54% as shown in Table 2. This phenomenon also can be confirmed in device 5 as shown in Figure 1(b) and Table 2. Accordingly, these results demonstrated that the significant enhancement in V_{OC} and PCE for the $CH_3NH_3PbI_3$/C_{60} or derivatives could be obtained not only from the

energy level offset between of HOMO level of donor ($CH_3NH_3PbI_3$ perovskite) and the LUMO level of acceptor (C_{60} or PCBM) but also the selective positive electrode with the larger work function. It is impressive that V_{OC} of device 6 (1.06 V) using PCBM as acceptor and ITO-2 as positive electrode was much higher than that of device 1 (0.6 V) using C_{60} as acceptor and ITO-1 as positive electrode. It is the first time that the highest V_{OC} of 1.06 V and PCE of 4.54% were achieved in the planar $CH_3NH_3PbI_3$-based PHJ on flexible substrates.

To investigate other influences of these two ITOs electrode on the enhanced photovoltaic performance in the device 2, the optical property of ITO-1 and ITO-2 was measured by UV-vis spectrometer. Figure 3 presents the transmission spectra of the ITO-1 and ITO-2 substrate. It can be observed that the transmittance of the ITO-1 is similar to the ITO-2 up to 80% at UV-vis to near-IR wavelength. However, there is a slightly redshift on the transmission toward the visible range for ITO-2. The transmission loss in ITO-2 cuts off the IPCE response in the blue part as shown in Figure 4, where we do observe inferior photon to electron conversion ability in the short wavelength region (< 450 nm). Furthermore, the enhanced J_{SC} and PCE can be proved in the measured IPCE response as shown in Figure 4. In Figure 4, the maximum peak of 43% at 500 nm in device 7 higher than that in device 5 agrees with the photovoltaic performance in Figure 1(b) and Table 2. It is interesting to highlight that devices using ITO-2 not only yielded high voltage but current as well. This is probably due to the large work function difference between the two contact materials that provides a stronger electrical field across the photoactive layer, thus an enhanced driving force for charge collection. Alternatively, if we view the perovskite material as an intrinsic semiconductor with Fermi level positioned near the middle of the band-gap, the high work function ITO will form a Schottky barrier with perovskite. This band offset acts as a surface field, which reduces the charge recombination at the

contact interface and might be advantageous for current collection.

Obviously, the light harvesting efficiency in our thin absorber is still far from the optimal scenario. Improvement on thin film deposition route for thicker film (> 100nm) is expected to increase the performance. Energy level engineering of contact materials or surface modification of electrode shall be effective to further enlarge V_{OC}, charge separation and collection. These topics are future works to be address for improving this type of planar junction device. During the preparation of this manuscript, we are aware of a very recent accomplishment on a mesoscopic sensitization-type flexible device with efficiency of 2.62%.[55] Our results showed that even in an extra-thin OPV-like bilayer structure, flexible perovskite devices could still aim higher for their photovoltaic performances. We believe the low temperature process of this device architecture is advantageous for cost-affordable photovoltaics and tandem design with other solar cells.

Conclusion

In conclusion, we have successfully demonstrated the fabrication of the all-solid-state, hybrid, donor–acceptor, $CH_3NH_3PbI_3$ perovskite/C_{60} PHJ solar cells under low temperature on flexible substrate with tunable V_{OC}. We study the effects of the contact material energy matching with the organometal halide perovskites material on the photovoltaic response of bilayer donor-acceptor type extremely thin absorber (ETA) solar cells. Applying ITO substrates with different work functions, we can achieve the higher V_{OC} to enhance the PCE of device. The higher work function of PET/ITO substrate leads the smaller energy loss for charge collection between the selective contact (ITO) and absorber (perovskite). By changing the work function of ITO layer, we can minimize the energy loss at the interface between perovskite and

ITO that resulted in the improved output voltage and overall power conversion efficiency. The V_{OC} increases significantly to more than 0.9 V with efficiency enhanced to 4.54 % compared to our previous published results (0.6 V and 3.9%). Our results represent the guidelines to systematically improve this type of ETA bilayer junction photovoltaic device and a promising process for low-cost photovoltaic devices.

"Note added in proof: During the revision of this paper, some highly relevant articles to this topic was published:

1. P. Docampo, J. M. Ball, M. Darwich, G. E. Eperon and H. J. Snaith, "Efficient organometal trihalide perovskite planar-heterojunction solar cells on flexible polymer substrate" *Nat. Commun.*, 2013, **4**, 2761.
2. D. Liu and T. L. Kelly, "Perovskite solar cells with a planar heterojunction structure prepared using room-temperature solution processing techniques" *Nat. Photon.*, Published online: 22 December 2013, doi:10.1038/nphoton.2013.342
3. J. You, Z. Hong, Y. (Michael) Yang, Q. Chen, M. Cai, T. B. Song, C. C. Chen, S. Lu, Y. Liu, H. Zhou and Y. Yang, "Low-temperature solution-processed perovskite solar cells with high efficiency and flexibility, *ACS Nano*, Published online: 5 January 2014, doi:10.1021/nn406020d

Acknowledgements

P. Chen thanks the financial support from the National Science Council (NSC) of Taiwan (NSC102-2113-M-006-010). The author, T.–F. Guo, would like to thank the National Science Council (NSC) of Taiwan (NSC102-2682-M-006-001-MY3) for financially supporting this research. Funding from the Research Center for Energy Technology and Strategy (RCETS) and the Advanced Optoelectronic Technology Center (AOTC) of National Cheng Kung University are acknowledged.

Reference:

1. B. O'Regan and M. Grätzel, *Nature*, 1991, **353**, 737-740.
2. A. Yella, H.-W. Lee, H. N. Tsao, C. Yi, A. K. Chandiran, M. K. Nazeeruddin, E. W.-G. Diau, C.-Y. Yeh, S. M. Zakeeruddin and M. Grätzel, *Science*, 2011, **334**, 629-634.
3. M. C. Scharber and N. S. Sariciftci, *Prog. Polym. Sci.*, 2013, **38**, 1929–1940.
4. M. Graetzel, R. A. J. Janssen, D. B. Mitzi and E. H. Sargent, *Nature*, 2012, **488**, 304-312.
5. C. R. Kagan, D. B. Mitzi and C. D. Dimitrakopoulos, *Science*, 1999, **286**, 945-947.
6. A. Kojima, K. Teshima, Y. Shirai and T. Miyasaka, *J. Am. Chem. Soc.*, 2009, **131**, 6050-6051.
7. H.-S. Kim, C.-R. Lee, J.-H. Im, K.-B. Lee, T. Moehl, A. Marchioro, S.-J. Moon, R. Humphry-Baker, J.-H. Yum, J. E. Moser, M. Grätzel and N.-G. Park, *Sci. Rep.*, 2012, **2**, 591.
8. M. M. Lee, J. Teuscher, T. Miyasaka, T. N. Murakami and H. J. Snaith, *Science*, 2012, **338**, 643-647.
9. J. Burschka, N. Pellet, S.-J. Moon, R. Humphry-Baker, P. Gao, M. K. Nazeeruddin and M. Grätzel, *Nature*, 2013, **499**, 316-319.
10. M. Liu, M. B. Johnston and H. J. Snaith, *Nature*, 2013, **501**, 395–398.
11. J. H. Heo, S. H. Im, J. H. Noh, T. N. Mandal, C.-S. Lim, J. A. Chang, Y. H. Lee, H.-J. Kim, A. Sarkar, M. K. Nazeeruddin, M. Grätzel and S. I. Seok, *Nature Photon.*, 2013, **7**, 487-492.
12. J. M. Ball, M. M. Lee, A. Hey and H. J. Snaith, *Energy Environ. Sci.*, 2013, **6**, 1739-1743.
13. J. H. Noh, S. H. Im, J. H. Heo, T. N. Mandal and S. I. Seok, *Nano Lett.*, 2013, **13**, 1764-1769.
14. W. Shockley and H. J. Queisser, *J. Appl. Phys.*, 1961, **32**, 510–519.
15. M. Hirasawa, T. Ishihara, T. Goto, K. Uchida and N. Miura, *Physica B* 1994, **201**, 427-430.
16. T. Ishihara, *J. Lumin.*, 1994, **60-61**, 269.
17. K. Tanaka, T. Takahashi, T. Ban, T. Kondo, K. Uchida and N. Miura, *Solid State Commun.* , 2003, **127**, 619-623.
18. J.-H. Im, C.-R. Lee, J.-W. Lee, S.-W. Park and N.-G. Park, *Nanoscale*, 2011, **3**, 4088-4093.
19. N.-G. Park, *J. Phys. Chem. Lett.* , 2013, **4**, 2423-2427.
20. B. Cai, Y. Xing, Z. Yang, W.-H. Zhang and J. Qiu, *Energy Environ. Sci.*, 2013, **6**, 1480-1485.

21. E. Edri, S. Kirmayer, D. Cahen and G. Hodes, *J. Phys. Chem. Lett.*, 2013, **4**, 897-902.
22. D. Bi, L. Yang, G. Boschloo, A. Hagfeldt and E. M. J. Johansson, *J. Phys. Chem. Lett.*, 2013, **4**, 1532-1536.
23. H.-S. Kim, I. Mora-Sero, V. Gonzalez-Pedro, F. Fabregat-Santiago, E. J. Juarez-Perez, N.-G. Park and J. Bisquert, *Nat. Commun.*, 2013, **4**.
24. D. Bi, S.-J. Moon, L. Haggman, G. Boschloo, L. Yang, E. M. J. Johansson, M. K. Nazeeruddin, M. Gratzel and A. Hagfeldt, *RSC Advances*, 2013, **3**, 18762-18766.
25. G. E. Eperon, V. M. Burlakov, P. Docampo, A. Goriely and H. J. Snaith, *Adv. Funct. Mater.*, 2013, **online published** DOI: 10.1002/adfm.201302090.
26. L. Etgar, P. Gao, Z. Xue, Q. Peng, A. K. Chandiran, B. Liu, M. K. Nazeeruddin and M. Graetzel, *J. Am. Chem. Soc.*, 2012, **134**, 17396-17399.
27. W. A. Laban and L. Etgar, *Energy Environ. Sci.*, 2013, **6**, 3249-3253.
28. J.-Y. Jeng, Y.-F. Chiang, M.-H. Lee, S.-R. Peng, T.-F. Guo, P. Chen and T.-C. Wen, *Adv. Mater.*, 2013, **25**, 3727-3732.
29. H.-S. Kim, J.-W. Lee, N. Yantara, P. P. Boix, S. A. Kulkarni, S. Mhaisalkar, M. Graetzel and N.-G. Park, *Nano Lett.*, 2013, **13**, 2412-2417.
30. D. Bi, G. Boschloo, S. Schwarzmuller, L. Yang, E. M. J. Johansson and A. Hagfeldt, *Nanoscale*, 2013, **5**.
31. J. Qiu, Y. Qiu, K. Yan, M. Zhong, C. Mu, H. Yan and S. Yang, *Nanoscale*, 2013, **5**, 3245-3248.
32. D. Sabba, H. M. Kumar, N. Yantara, T. T. T. Pham, N.-G. Park, M. Gratzel, S. G. Mhaisalkar, N. Mathews and P. P. Boix, *Nanoscale*, 2014, **6**, 1675-1679
33. P. K. Nayak, J. Bisquert and D. Cahen, *Adv. Mater.*, 2011, **23**, 2870-2876.
34. V. Shrotriya, G. Li, Y. Yao, T. Moriarty, K. Emery and Y. Yang, *Adv. Funct. Mater.*, 2006, **16**, 2016-2023.
35. C. Waldauf, M. C. Scharber, P. Schilinsky, J. A. Hauch and C. J. Brabec, *J. Appl. Phys.*, 2006, **99**, 104503-104506.
36. G. Xing, N. Mathews, S. Sun, S. S. Lim, Y. M. Lam, M. Grätzel, S. Mhaisalkar and T. C. Sum, *Science*, 2013, **342**, 344-347.
37. S. D. Stranks, G. E. Eperon, G. Grancini, C. Menelaou, M. J. P. Alcocer, T. Leijtens, L. M. Herz, A. Petrozza and H. J. Snaith, *Science*, 2013, **342**, 341-344.
38. C. J. Brabec, A. Cravino, D. Meissner, N. S. Sariciftci, T. Fromherz, M. T. Rispens, L. Sanchez and J. C. Hummelen, *Adv. Funct. Mater.*, 2001, **11**, 374-380.
39. V. D. Mihailetchi, P. W. M. Blom, J. C. Hummelen and M. T. Rispens, *J. Appl.*

Phys., 2003, **94**, 6849-6854.
40. A. Manor and E. A. Katz, *Sol. Energy Mater. Sol. Cells*, 2012, **97**, 132-138.
41. R. A. J. Janssen and J. Nelson, *Adv. Mater.*, 2013, **25**, 1847-1858.
42. M. C. Scharber, D. Mühlbacher, M. Koppe, P. Denk, C. Waldauf, A. J. Heeger and C. J. Brabec, *Adv. Mater.*, 2006, **18**, 789-794.
43. M. F. Lo, T. W. Ng, T. Z. Liu, V. A. L. Roy, S. L. Lai, M. K. Fung, C. S. Lee and S. T. Lee, *Appl. Phys. Lett.*, 2010, **96**, 113303.
44. L.-M. Chen, Z. Xu, Z. Hong and Y. Yang, *J. Mater. Chem.*, 2010, **20**, 2575-2598.
45. V. D. Mihailetchi, L. J. A. Koster and P. W. M. Blom, *Appl. Phys. Lett.*, 2004, **85**, 970.
46. C. J. Brabec, S. E. Shaheen, C. Winder, N. S. Sariciftci and P. Denk, *Appl. Phys. Lett.*, 2002, **80**, 1288-1290.
47. A. Gadisa, M. Svensson, M. R. Andersson and O. Inganas, *Appl. Phys. Lett.*, 2004, **84**, 1609-1611.
48. J. Liu, Y. Shi and Y. Yang, *Adv. Funct. Mater.*, 2001, **11**, 420-424.
49. J. H. Noh, N. J. Jeon, Y. C. Choi, M. K. Nazeeruddin, M. Grätzel and S. I. Seok, *J. Mater. Chem. A*, 2013, **1**, 11842-11847.
50. H. Ishii, K. Sugiyama, E. Ito and K. Seki, *Adv. Mater.*, 1999, **11**, 605-625.
51. G. Liu, W. Jaegermann, J. He, V. Sundström and L. Sun, *J. Phys. Chem. B*, 2002, **106**, 5814-5819.
52. E. L. Ratcliff, A. Garcia, S. A. Paniagua, S. R. Cowan, A. J. Giordano, D. S. Ginley, S. R. Marder, J. J. Berry and D. C. Olson, *Adv. Energy Mater.*, 2013, **3**, 647-656.
53. G. Li, R. Zhu and Y. Yang, *Nature Photon.*, 2012, **6**, 153-161.
54. B. E. Hardin, H. J. Snaith and M. D. McGehee, *Nature Photon.*, 2012, **6**, 162-169.
55. M. H. Kumar, N. Yantara, S. Dharani, M. Graetzel, S. Mhaisalkar, P. P. Boix and N. Mathews, *Chem. Comm.*, 2013, **49**, 11089-11091.

Table 1

Recent photovoltaic devices based on organometallic perovskite material with their junction structures, function of perovskite and photovoltaic performances.

Device structure	Function of Perovskite	V_{OC} (mV), J_{SC} (mA/cm^2) Efficiency (%)	V_{OC} / E_g (%)
TiO_2 (nc)/$CH_3NH_3PbI_3$/*spiro*-OMeTAD/Au[7]	A + ETM	888, 17.6, 9.7	59.2
TiO_2 (nc)/$CH_3NH_3PbI_3$/PTAA/Au[11]	A+ ETM	997, 16.5, 12.0	64.4
Al_2O_3(nc)/$CH_3NH_3PbI_2Cl$/*spiro*-OMeTAD/Ag[8]	A+ ETM	980, 17.8, 10.9	63.2
TiO_2 (nc)/$CH_3NH_3PbI_2Cl$/*spiro*-OMeTAD/Ag[8]	A+ ETM	800, 17.8, 7.8	51.6
TiO_2 (TF)/$CH_3NH_3PbI_2Cl$/*spiro*-OMeTAD/Ag[8]	A+ ETM	640, 7.13, 1.8	41.3
TiO_2 (nc)/$CH_3NH_3PbI_3$/*spiro*-OMeTAD/Au[9]	A + ETM	993, 20.0, 15.0	64.4
TiO_2 (TF)/$CH_3NH_3PbI_2Cl$/*spiro*-OMeTAD/Ag[10]	A + ETM	1070, 21.5, 15.4	69.0
ITO/PEDOT/$CH_3NH_3PbI_3$/PCBM/Al[28]	A + HTM	600, 10.32, 3.9	38.7
TiO_2 (sht)/$CH_3NH_3PbI_3$/Au[26]	A + HTM	630, 16.1, 5.5	40.6
ITO/PEDOT/$CH_3NH_3PbI_3$/PCBM/Al*	A + HTM	920, 7.93, 4.54	61.3

Note: nc: nanocrystalline, A: absorber, ETM: electron transport material, HTM: hole transport material, TF: thin film, sht: sheet. *: current work.

Table 2 Photovoltaic parameters of perovskite/acceptor-based solar cells of different acceptor layers and ITO substrates.

Device	V_{OC} (V)	J_{SC} (mA/cm^2)	FF	PCE (%)	R_S (ohm*cm^2)	R_P (Mohm)
Device 1: perovskite/C_{60}(30nm) (ITO-1)	0.60	6.12	0.52	1.93	1.93	2.91
Device 2: perovskite/C_{60}(30nm) (ITO-2)	0.84	8.18	0.53	3.62	6.09	33.24
Device 3: perovskite/C_{60}(30nm) (Ni-ITO)	0.80	6.20	0.51	2.51	6.99	10.58
Device 4: perovskite/PCBM(30nm) (ITO-1)	0.75	4.80	0.59	2.12	6.12	62.81
Device 5: perovskite/PCBM(20nm) (ITO-1)	0.68	6.57	0.69	3.10	2.44	1.44
Device 6: perovskite/PCBM(30nm) (ITO-2)	1.06	6.20	0.47	3.13	18.76	80.48
Device 7: perovskite/PCBM(20nm) (ITO-2)	0.92	7.93	0.62	4.54	8.60	1.43

Scheme 1. (a) Energy diagram of device applying PCBM as the acceptor; (b) Photo of perovskite PHJ solar cell on flexible PET/ITO substrate and device architecture of the perovskite PHJ solar cell.

(a)

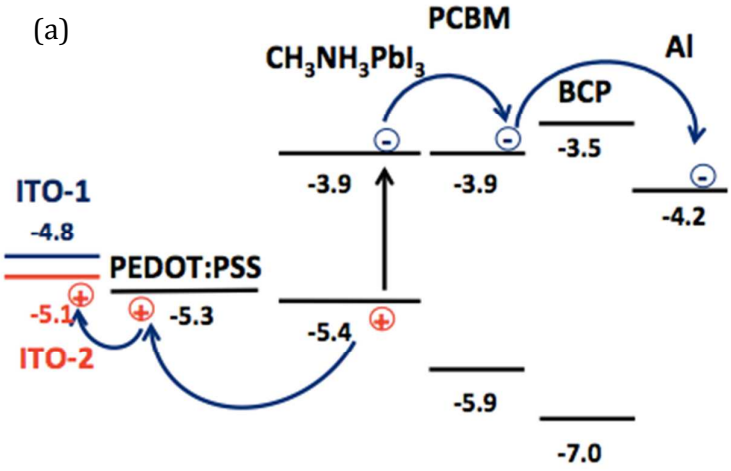

(b)

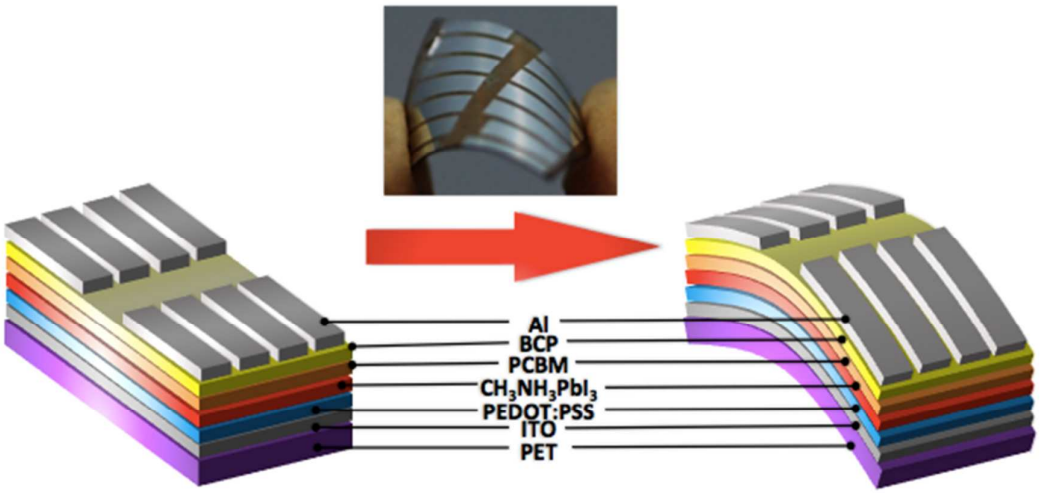

Figure Captions

FIGURE 1. (a) *J-V* curves of $CH_3NH_3PbI_3$ perovskite (γ-butyrolactone)/C_{60} (30 nm) on glass/ ITO (ITO-1) (●), PET ITO (ITO-2) (■) and glass/ ITO/nickel-doped ITO (Ni-ITO) substrates (◆). (b) *J-V* curves of $CH_3NH_3PbI_3$ perovskite (γ-butyrolactone)/PCBM hybrid solar cells: perovskite/PCBM (30 nm) on ITO-1 (▼), perovskite/PCBM (20 nm) on ITO-1 (◆), perovskite/PCBM (30 nm) on ITO-2 (●), and perovskite/PCBM (20 nm) on ITO-2 (■) substrates under standard 1 Sun AM 1.5 G simulated solar irradiation.

FIGURE. 2. UPS (He I) for the surface measurement of glass/ITO (ITO-1) (●) and PET/ITO (ITO-2) (■) substrates. The two inset figures on the top present the details of the onset (E_i) and cut-off ($E_{cut\text{-}off}$) energy regions for the UPS measurement.

FIGURE. 3. UV-vis absorbance spectrum of $CH_3NH_3PbI_3$ perovskite layers prepared from γ-butyrolactone (6000 rpm) solution 14.9 wt% on quartz/PEDOT:PSS substrates (◆), transmission spectra of ITO-1 (●) and ITO-2 (■) substrates.

FIGURE .4. IPCE spectra of device 5: perovskite/PCBM (20 nm) on ITO-1 substrate (●), and device 7: perovskite/PCBM (20 nm) on ITO-2 (■) substrate.

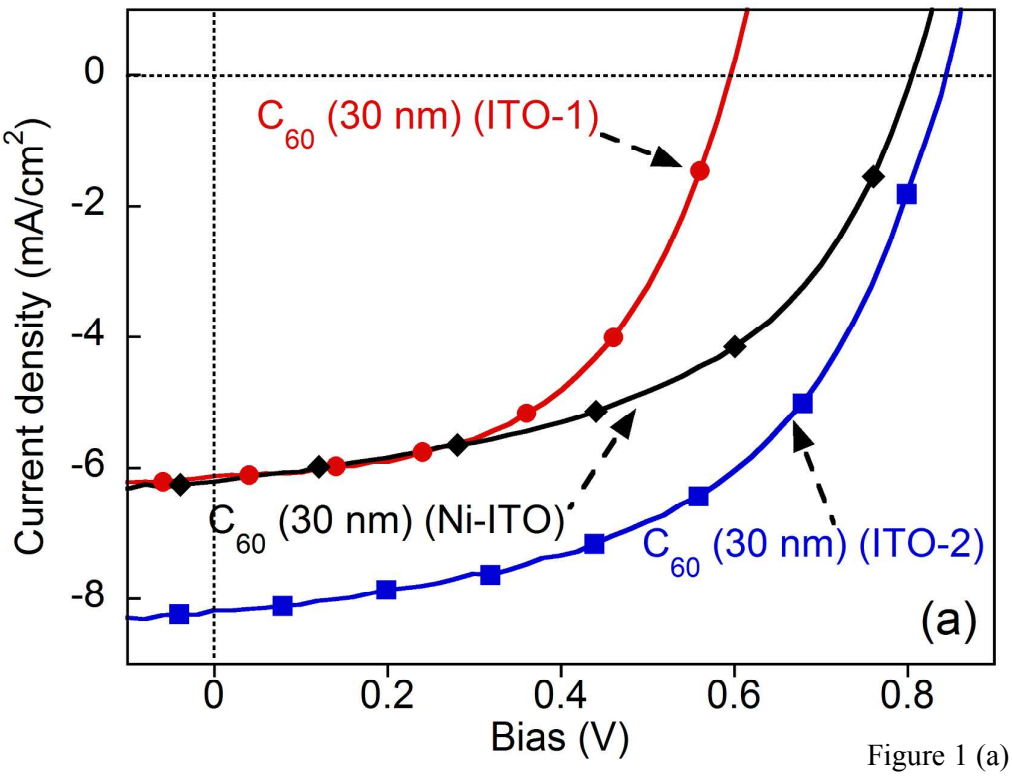

Figure 1 (a)

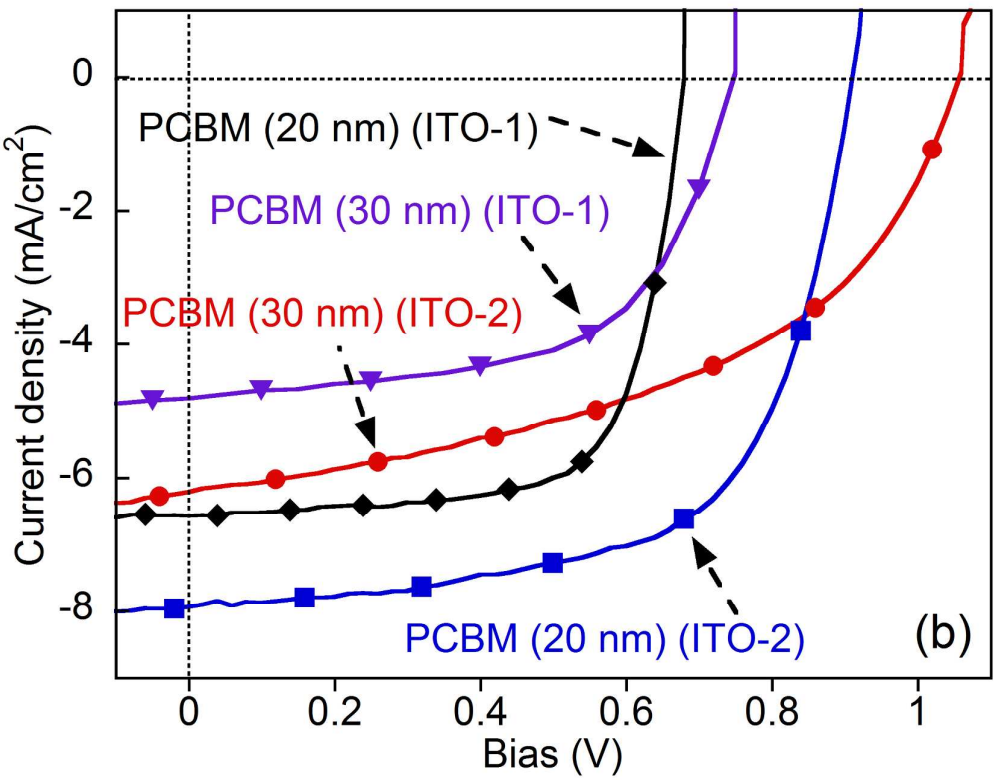

Figure 1 (b)

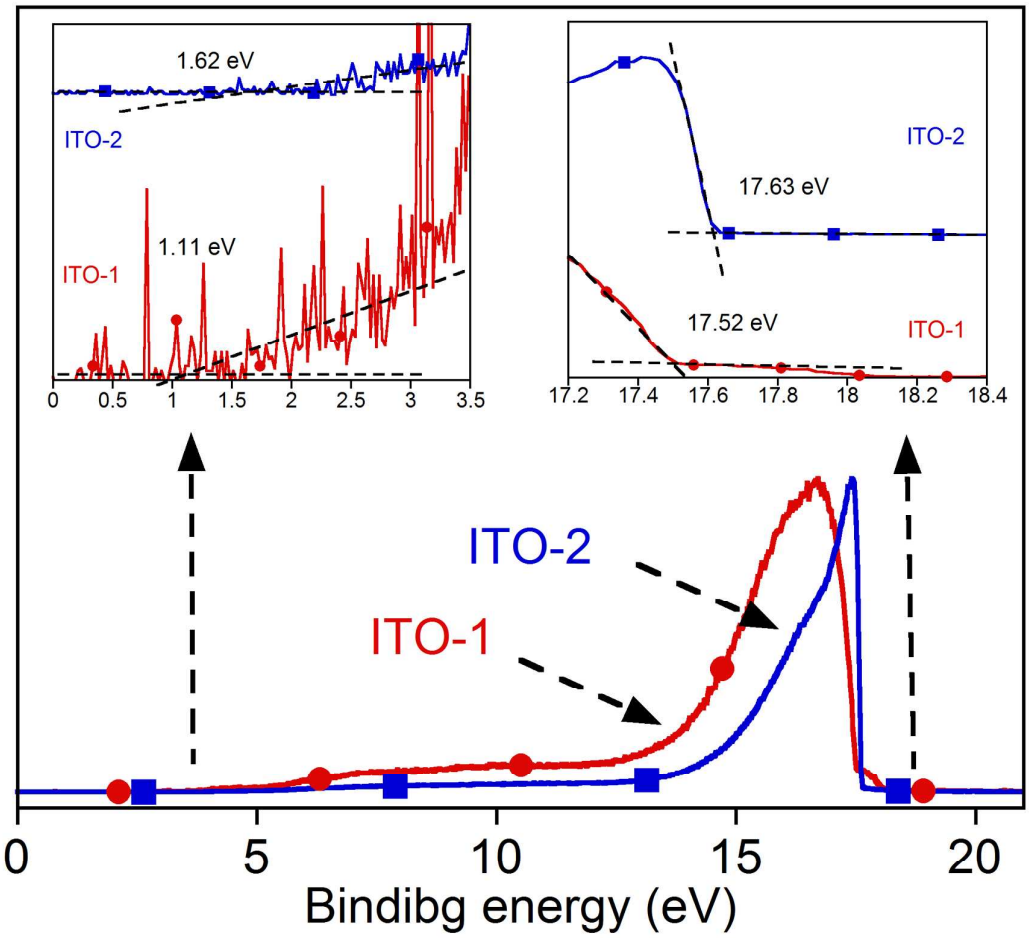

Figure 2

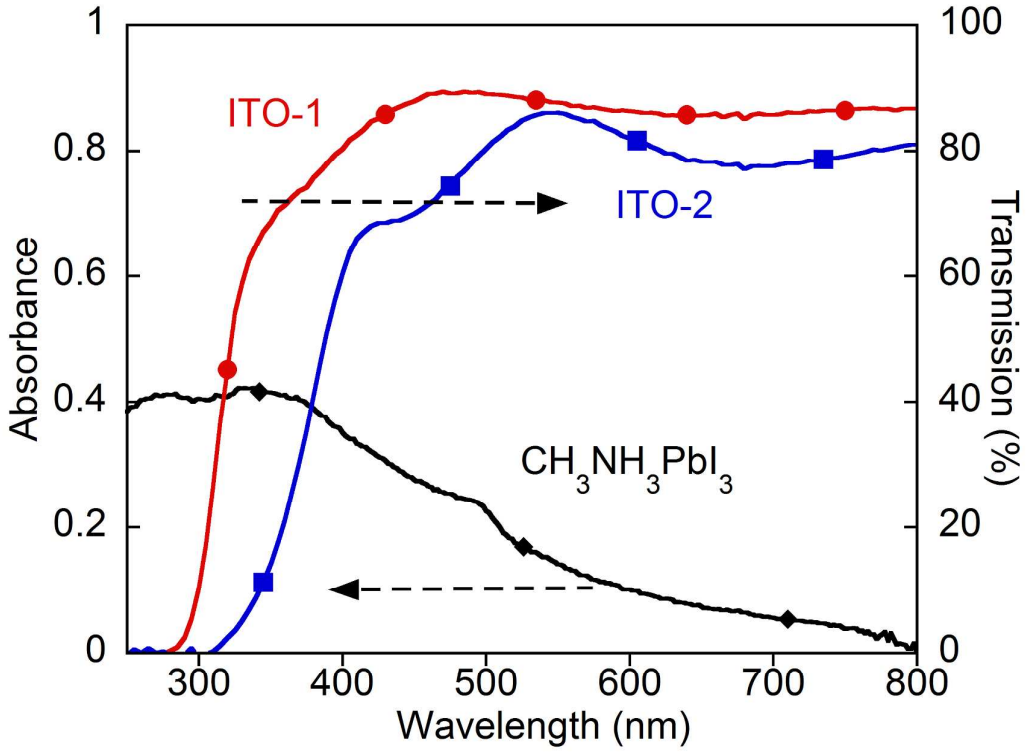

Figure 3

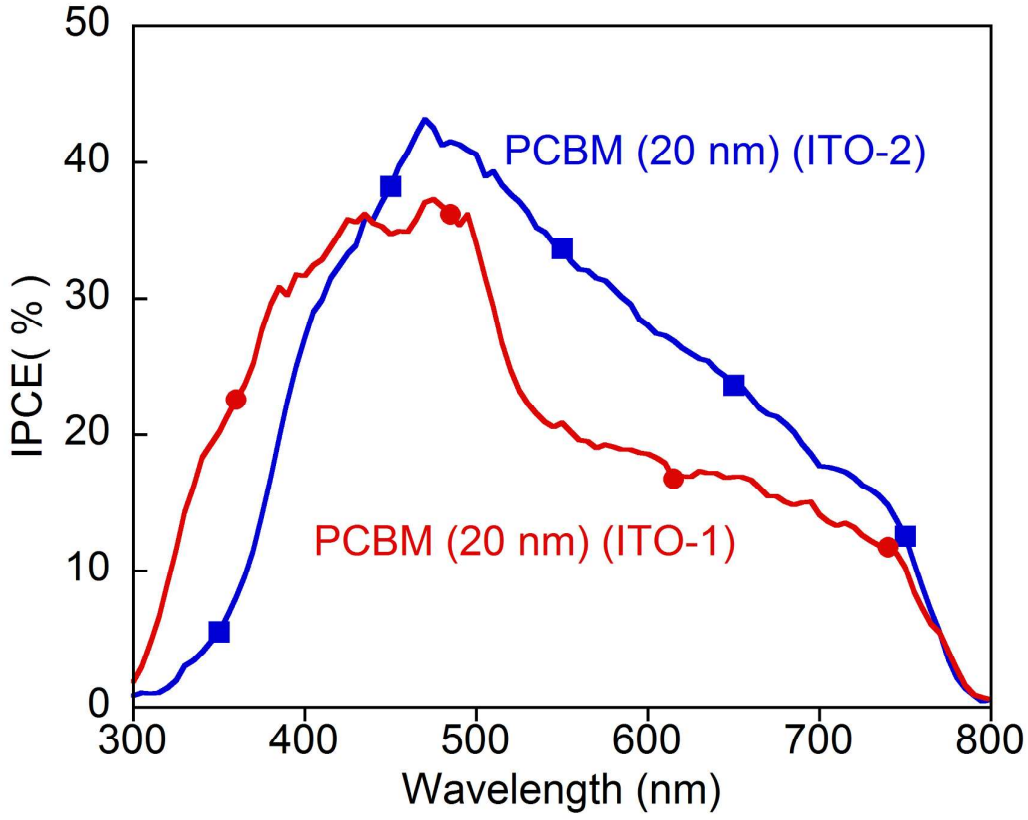

Figure 4